

EFFECTS OF FIN LENGTH AND FIN VALLEY ON THE PERFORMANCE OF BUS DUCT CONDUCTOR

By:

HOOI KHEY HERNG

(Matrix no.: 142809)

Supervisor:

Dr. Mohd Sharizal Bin Abdul Aziz

July 2022

This dissertation is submitted to

Universiti Sains Malaysia

As partial fulfillment of the requirement to graduate with honors degree in

BACHELOR OF ENGINEERING (MECHANICAL ENGINEERING)



School of Mechanical Engineering

Engineering Campus

Universiti Sains Malaysia

DECLARATION

This work has not previously been accepted in substance for any degree and is not being concurrently submitted in candidature for any degree.

Signed.......... (HOOI KHEY HERNG)

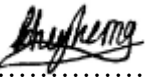
Date..... 15/7/2022

STATEMENT 1

This thesis is the result of my own investigations, except where otherwise stated.

Other sources are acknowledged by giving explicit references.

Bibliography/references are appended.

Signed.......... (HOOI KHEY HERNG)

Date..... 15/7/2022

STATEMENT 2

I hereby give consent for my thesis, if accepted, to be available for photocopying and for interlibrary loan, and for the title and summary to be made available outside organizations.

Signed.......... (HOOI KHEY HERNG)

Date..... 15/7/2022

ACKNOWLEDGEMENT

First and foremost, I would like to express my special thanks of gratitude to my beloved university, Universiti Sains Malaysia (USM), especially the School of Mechanical Engineering for giving me the opportunity to use the tools and equipment in CAD lab. I am provided with computer, air-conditioner and stable internet connection, which enable us to work in a very comfortable environment with high efficiency in CAD lab.

In addition, I would like to thank Furutec Electrical Sdn. Bhd. for allowing me involved in this industry project. The company provides the bus duct prototype so that the experiment can be carried out successfully.

Besides that, my sincere thanks also go to my supervisor, Dr. Mohd Sharizal Bin Abdul Aziz for his able guidance and support in completing my final year project. He always gives me moral supports and guide me on how to do the project in purpose to produce a good outcome from theories and knowledge that been studied.

Next, I would also like to thank the coordinator of this course, Dr. Muhammad Fauzinizam Bin Razali for spending his valuable time teaching us the theories and knowledge of this course. I would also like to thank Mr. Mark Selvan in guiding me throughout familiarizing with the ANSYS software and producing the desired outcomes. My completion of this project could not have been accomplished without his guidance and support.

Furthermore, I would like to thank all the technical staff for their active cooperation in supporting and guiding me throughout the project. I owe a gratefulness to my friends for all the ways they inspired, supported, and encouraged me to finish this project.

TABLE OF CONTENTS

DECLARATION.....	ii
ACKNOWLEDGEMENT.....	iii
TABLE OF CONTENTS	iv
LIST OF TABLES	vi
LIST OF FIGURES	vii
LIST OF ABBREVIATIONS	x
ABSTRAK	xi
ABSTRACT.....	xii
CHAPTER 1 INTRODUCTION.....	1
1.1 Overview of Project	1
1.2 Problem Statement	3
1.3 Objectives.....	3
1.4 Scope of Project	3
CHAPTER 2 LITERATURE REVIEW.....	5
2.1 Overview	5
2.2 Computational Fluids Dynamic (CFD) in Thermal Analysis	5
2.3 Transient Thermal Analysis	6
2.4 Finite Element in Fluid	7
2.5 Finite Volume for Fluid Flow	9
2.6 Bus Duct Design	11
2.7 Summary	13
CHAPTER 3 METHODOLOGY.....	14
3.1 Overview	14
3.2 Mathematical Equations.....	15

3.3	Computational Approach	18
3.3.1	Pre-processing	18
3.3.1(a)	Geometrical Model	18
3.3.1(b)	Meshing	19
3.3.2	Computational Setup.....	21
3.3.2(a)	Boundary Conditions Setup.....	22
3.3.2(b)	Run Calculation Setup.....	23
3.3.3	Post-processing	24
3.3.3(a)	Thermal Performance of Heatsink.....	24
3.3.3(b)	Contours Setup	26
3.4	Experimental Validation	28
CHAPTER 4 RESULTS AND DISCUSSION		31
4.1	Overview	31
4.2	Mesh Independence Test.....	31
4.3	Experimental Validation	33
4.4	Simulation Results	35
4.4.1	Effect of Fin Length on Performance of Heatsink.....	35
4.4.2	Effect of Fin Valley on Performance of Heatsink.....	42
4.5	Limitations	48
CHAPTER 5 CONCLUSION AND FUTURE WORK		49
5.1	Conclusion	49
5.2	Recommendations for Future Research	49
REFERENCES.....		51
APPENDIX A	PROPERTIES OF MATERIAL	57
APPENDIX B	CAD MODEL OF HEATSINK.....	59
APPENDIX C	GANTT CHART.....	65

LIST OF TABLES

Table 2.1	Comparison of experimental data and simulation data of the fins at 8 different fin instances.....	6
Table 3.1	IEC 61439-6 temperature rise specifications.....	28
Table 4.1	Mesh independence test results.....	31
Table 4.2	Thermal performance of different fin length.....	35
Table 4.3	Thermal performance of different fin valleys.....	42

LIST OF FIGURES

Figure 2.1	Temperature distributions of the solution regions. (a) Single-phase bus bar. (b) Three-phase bus bar.....	7
Figure 2.2	Fluid field the solution regions. (a) Single-phase bus bar. (b) Three-phase bus bar.....	8
Figure 2.3	Temperature distribution of a single-phase bus bar model.....	9
Figure 2.4	Result comparison between experiment and simulations	10
Figure 2.5	Fins with different geometrics [23].....	11
Figure 2.6	Schema of triangular fin along with the different perforations [23]..	11
Figure 3.1	Flow chart of simulation setup.....	14
Figure 3.2	Dimension and Geometrical Setup	18
Figure 3.3	Surface mesh setup showing minimum surface mesh size was set at 0.0001573 with a growth rate of 1.2.....	19
Figure 3.4	Volume mesh setup showing the volume mesh is filled with poly-hexcore cells.....	20
Figure 3.5	Mesh grid and three boundary layers details around heat sink	20
Figure 3.6	General setup showing pressure-based solver with transient time	21
Figure 3.7	Boundary conditions and cell zone conditions	23
Figure 3.8	Run calculation setup showing the parameter with 20000 time steps and 0.1 time step size	23
Figure 3.9	Flux reports showing total heat transfer rate was chosen and “fluid-domain-heatsink” was filtered to choose the shadow.....	24
Figure 3.10	Wall zone name showing the adjacent cell zone was heatsink.....	25
Figure 3.11	Load Results showing the cdat file at 2000 seconds was selected	25
Figure 3.12	New Expression Created for Thermal Performance of Heatsink.....	26
Figure 3.13	Plane 1 showing the ZX plane with Y-coordinate of 0.001535 m.....	26

Figure 3.14	Temperature contour setting	27
Figure 3.15	Velocity vector contour setting.....	27
Figure 3.16	Schematic diagram of experimental setup	29
Figure 3.17	Experimental setup showing setup 1m from the floor and ambient temperature recorded 1m away from the casing using K-type thermocouple.....	29
Figure 3.18	Heatsink experiment model	30
Figure 3.19	(a) Incoming portion (b) Outgoing portion.....	30
Figure 4.1	Mesh independence plot showing total heat transfer rate against number of elements for different mesh sizes	32
Figure 4.2	Temperature rise of bus duct conductor for experimental setup.....	33
Figure 4.3	Graph of fin tip temperature against time of simulation result.....	34
Figure 4.4	Graph of fin tip temperature against experimental result and simulation result.....	34
Figure 4.5	Graph of volume of heatsink against fin length.....	36
Figure 4.6	Graph of average surface temperature and fin effectiveness against fin length	37
Figure 4.7	Graph of average surface heat transfer coefficient and total heat transfer rate against fin length.....	37
Figure 4.8	Graph of average surface Nusselt number against fin length	38
Figure 4.9	Temperature contour heatsink with (a) 5 mm fin length (b) 6.5 mm fin length	39
Figure 4.10	Velocity vector contour of 5.0 mm fin length heatsink	39
Figure 4.11	Velocity vector contour of 6.5 mm fin length heatsink	40
Figure 4.12	Graph of volume increment and total heat transfer rate increment against fin length.....	41
Figure 4.13	Graph of surface area of heatsink against fin valley	43

Figure 4.14	Graph of average surface temperature and fin effectiveness against fin valley	44
Figure 4.15	Graph of average surface heat transfer coefficient and total heat transfer rate against fin valley	44
Figure 4.16	Graph of average surface Nusselt number against fin valley	45
Figure 4.17	Temperature contour heatsink with (a) 5 fin valleys (b) 6 fin valleys	46
Figure 4.18	Velocity vector contour of 5 fin valleys heatsink	46
Figure 4.19	Velocity vector contour of 6 fin valleys heatsink	47
Figure 4.20	Graph of surface area increment and total heat transfer rate increment against fin length.....	48

LIST OF ABBREVIATIONS

USM	Universiti Sains Malaysia
CFD	Computational Fluid Dynamics
GSM	Gradient Smoothed Method
FEM	Finite Element Method
FVM	Finite Volume Method
PDE	Partial Differential Equation
SERC	Science and Engineering Research Centre
FSI	Fluid-Structure Interaction

KESAN KEPANJANGAN SIRIP DAN BILANGAN LEMBAH SIRIP TERHADAP PRESTASI KONDUKTOR SALURAN BAS

ABSTRAK

Terdapat banyak cara untuk mengalirkan elektrik dan salah satu kaedah alternatif penghantaran elektrik adalah dengan menggunakan konduktor saluran bas. Dalam sektor komersial dan perindustrian, konduktor saluran bas digunakan untuk membekalkan elektrik kepada kabel kuasa atau bas kabel. Walaubagaimanapun, permintaan untuk sink haba terma yang berprestasi tinggi semakin meningkat dan reka bentuk tradisional tidak lagi mencukupi. Justeru, objektif kajian ini adalah untuk menganalisis kesan kepanjangan sirip dan bilangan lembah sirip terhadap prestasi konduktor saluran bas dengan menggunakan Ansys Fluent. Berikut pengesahan keputusan simulasi dan eksperimen, keputusan menunjukkan ia mempunyai perbezaan peratusan sebanyak 4.57 %. Lima kepanjangan sirip yang berbeza (4.0 mm, 4.5 mm, 5.5 mm, 6.0 mm dan 6.5 mm) dan lima lembah sirip yang berbeza (2, 3, 4, 5 dan 6) digunakan dalam simulasi berangka ini. Keputusan menunjukkan bahawa purata suhu permukaan, jumlah kadar pemindahan haba, keberkesanan sirip dan purata permukaan nombor Nusselt meningkat apabila kedua-dua kepanjangan sirip dan bilangan lembah sirip meningkat. Walaubagaimanapun, purata pekali pemindahan haba permukaan sink haba berkurangan disebabkan oleh daya geseran apabila panjang sirip meningkat tetapi purata pekali pemindahan haba permukaan heatsink meningkat disebabkan peningkatan keluasan permukaan terdedah apabila bilangan lembah sirip meningkat. Kesimpulannya, sirip yang lebih panjang dan bilangan lembah sirip yang lebih banyak akan memberikan prestasi terma yang lebih baik dalam konduktor saluran bas.

EFFECTS OF FIN LENGTH AND FIN VALLEY ON THE PERFORMANCE OF BUS DUCT CONDUCTOR

ABSTRACT

There are many ways to conduct electricity and one of the alternative methods of transmitting electricity is by using bus duct conductor. In commercial and industrial sectors, bus duct conductor is used to supply electricity to power cables or cable buses. However, the demand for high-performance thermal heat sinks is growing and conventional designs are no longer adequate. Hence, the objective of this study is to analyse the effects of fin length and fin valley on the performance of bus duct conductor using Ansys Fluent. Following the verification of the simulation and experiment results, the results showed that it had a percentage difference of 4.57 %. Five different fin length (4.0 mm, 4.5 mm, 5.5 mm, 6.0 mm and 6.5 mm) and five different fin valleys (2, 3, 4, 5 and 6) are used in this numerical simulation. The results demonstrated that the average surface temperature, total heat transfer rate, fin effectiveness and average surface Nusselt number increased when both fin length and fin valley increased. However, the average surface heat transfer coefficient of heatsink decreased due to frictional forces when fin length increased but the average surface heat transfer coefficient of heatsink increased due to increase of exposed surface area as the fin valley increased. In conclusion, longer fin length and higher number of fin valley will provide better thermal performance in bus duct conductor.

CHAPTER 1

INTRODUCTION

1.1 Overview of Project

Bus ducts also called as busways or busbar trunking systems are power distribution systems that use copper or aluminium busbars to transport electrical energy and are protected by an aluminium enclosure. They were utilised because they were more efficient and adequate to the job when large quantities of power were needed from electrical devices for industrial processes.

In most instances where cable or conduit would ordinarily be utilised, bus duct can be used instead. Many people mistakenly assume that bus duct is exclusively used for high-amperage applications. This is a common misconception as busways are quite efficient in both low- and high-amperage conditions. Bus duct systems come in a variety of sizes, from 100A to 6500A. High-tech enterprises, such as computer makers, might be examples of low-amperage applications. Heavy assembly sectors, such as automotive, need high-amperage busway systems [1].

Due to numerous significant benefits, bus ducts are steadily becoming more widespread as a power distribution system. The installation cost of a bus duct is affordable and saves money in the long term due to its rapid installation, ease of maintenance, and a longer lifetime. This is because they are faster to install compare to wires in runners, and their basic form allows for a lower margin of error. Due to the fact that bus ducts are less difficult to install compare to cables, less labour is needed. Moreover, maintenance expenses are reduced since they need less maintenance; once a year is adequate. Thirdly, a bus duct has an average lifetime of 20 years. The bus ducts can be altered at any moment, whether it is to add a new tap box or move the system itself, and components can be reused at any time. Since bus ducts are halogen-free, no

harmful fumes are emitted in the event of a fire. Additionally, the majority of the materials utilised are recyclable. Furthermore, if a new power connection is required, an extra plug-in unit can be inserted anywhere along the current open-access slot; plug-in units can also be customised or moved without causing any disruption to existing systems.

Heatsinks are used to efficiently disperse heat from a hot item to the environment via either forced or natural convection. Many sectors have invested much in research and development to reduce the total weight, area, and cost of incorporating heat sinks into electronics. In the design and development of high-performance thermal heat sinks, geometry is crucial. Many researches involving the design and usage of a bus bar for various purposes have been carried out. The bus bar's design and other important issues are often overlooked, with the focus being on reducing stray inductance.

In every simulation research, the grid independence test is critical. This ensures that the findings are unaffected by mesh size. Refer to research of Inthavong et al. [2], mesh independence based on the convergence of flow parameters on a single line is an unsatisfactory technique since the remainder of the domain is disregarded in the analysis of flow dynamics in the nasal cavity. As a consequence, certain mesh sections may be badly converged. Mesh independence based on a single averaged value of the global flow parameter, on the other hand, fails to account for locally inadequate mesh convergence. In a mesh independence test, both local and global flow parameters should be investigated.

1.2 Problem Statement

The usage of bus duct conductors in electric power distribution for factories and large buildings is well known. The demand for high-performance thermal heat sinks has beyond the capabilities of conventional designs. Hence, it is crucial to do research on maintaining a safe working temperature for electronic equipment. Besides, conducting laboratory tests will take a longer length of time. This is due to the fact that the prototype may need to be built and tested numerous times. Furthermore, there is a paucity of study on the performance of bus duct fin conductor in the literature. To solve these issues, obtaining a complete understanding of bus duct fin conductor is significant to engineers.

1.3 Objectives

The specific objectives of the project are:

- i. To analyse the impact of fin length on the thermal performance of a bus duct conductor using Computational Fluid Dynamics.
- ii. To study the impact of fin valley on the thermal performance of a bus duct conductor using Computational Fluid Dynamics.
- iii. To validate the simulation with experiment.

1.4 Scope of Project

Simulation will be required to finish the project. Five different fin length and fin valley are needed to analyse the impact of fin length and fin valley on the performance of the heatsink respectively. Various fin lengths were measured in 0.5 mm increments and decrements from the current geometry that is 5.0 mm. Hence, fin lengths of $l_1=4.0$ mm, $l_2=4.5$ mm, $l_3=5.5$ mm, $l_4=6.0$ mm, and $l_5=6.5$ mm were selected. On the other hand, number of fin valleys with $v_1=2$, $v_2=3$, $v_3=4$, $v_4=5$, and $v_5=6$ were

drawn. Fluent meshing will be used to mesh the geometry. The Mesh Independent Test was carried out to ensure that the simulation results are independent of the mesh resolution. The simulation model's cell zone and boundary conditions are set. Computational setup is set and ran with time step of 0.1 second and a 20000 number of time steps to model the heat transfer until steady state with no temperature changes on the heatsink. The data obtained from the simulation is statistically analysed to study the significant impact of fin length and fin valley on the performance of the heatsink respectively

The standard size of the bus duct conductor was designed, which included simulation and modelling of the bus duct conductor in order to validate its experiment results. The simulation and modelling will be carried out with the help of the ANSYS programme. The comparison between experimental and simulation results will be carried out to determine the verification of the simulation and experiment results.

CHAPTER 2

LITERATURE REVIEW

2.1 Overview

In this section, few topics are discussed to understand the current research and identify what is the unknown in these topics such as CFD in thermal analysis, transient thermal analysis, finite element in fluid, finite volume for fluid flow and the bus duct design.

2.2 Computational Fluids Dynamic (CFD) in Thermal Analysis

Computational fluid dynamics (CFD) is a topic of research concerned with using numerical simulations to analyse different kinds of fluid flows and creating appropriate simulation techniques [3]. CFD applications may be found in the following studies: flows surrounding aeroplanes, ships, trains, and vehicles, biomedical and biological fluxes. CFD analyses and predicts flow physics by numerically solving the governing equations and replicating the flow field using computers. The Eulerian representation, which defines the flow field using functions of space and time, and the Lagrangian representation, which describes the flow field following individual fluid components in the flow, are two formulations that can be used to describe fluid flow [4]. The air flow from the bus duct fin conductor can be modelled using a CFD model. According to the research from M. Selvan et al. [5], the created simulation model was tested using experimental data and found to have a divergence of around 5% as shown in Table 2.1. As a result, it can be utilised to investigate various geometrical patterns for future study using CFD.

Table 2.1 Comparison of experimental data and simulation data of the fins at 8 different fin instances

Position	Experimental Data	Simulation Data	Error (%)
1	84.8	88.65	4.54
2	84.6	88.81	4.97
3	84.9	88.71	4.49
4	84.8	88.80	4.71
5	84.7	88.62	4.62
6	85.1	88.75	4.29
7	85.0	88.73	4.39
8	84.9	88.77	4.56

2.3 Transient Thermal Analysis

J. Padet et al. [6] carried out a numerical investigation of the transient forced laminar convective heat transfer over a flat plate or a wedge when the thermal field is caused by time and space with specific boundary conditions. In a dense bed of spheres, transient heat transfer by free convection is modelled using two different methods by O. Laguerre et al. [7]. For a specific free convection setup, the numerical results produced using the two methodologies which are CFD software and porous medium approach are in good agreement with the experimental values of air and particle temperature. Jing Ma et al. [8] created and formulated spectral collocation approach to discuss transient thermal processes in a moving plate with temperature-dependent characteristics and heat generation. Result showed that increases of Peclet number will increase the heat transfer rate.

2.4 Finite Element in Fluid

Liu et al. [9][10] used the gradient smoothed method (GSM) by coupling meshfree approaches and the finite element method (FEM) approach. The fundamental concept behind the GSM is to build high-performing numerical models using a finite element mesh [11]. For the purpose of solving steady-state and transient incompressible fluid flow problems, Liu et al. created the GSM [12]. Since the suggested approach is based on irregular cells, it can be used to issues with geometrical borders of any complexity. Wu et al. [13] used FEM to perform the thermal analysis on both single-phase and three-phase bus bars. Based on Figure 2.1, the symmetric temperature distributions of the bus bars were shown at the ambient temperature of 21.5 °C. The movement of SF₆ gas and surrounding air is responsible for the temperature field distributions as shown in Figure 2.2. Due to its lower density, ambient air has a substantially greater velocity than SF₆ gas. Results showed the FEM fit well with measured values in single-phase bus bars but when it comes to three-phase bus bars, the difference in conductor temperatures between the FEM and analytical approaches is greater than 10% at 2 kA because the enclosure is isothermal and the convective heat transfer mechanism in three-phase bus bars is more complicated.

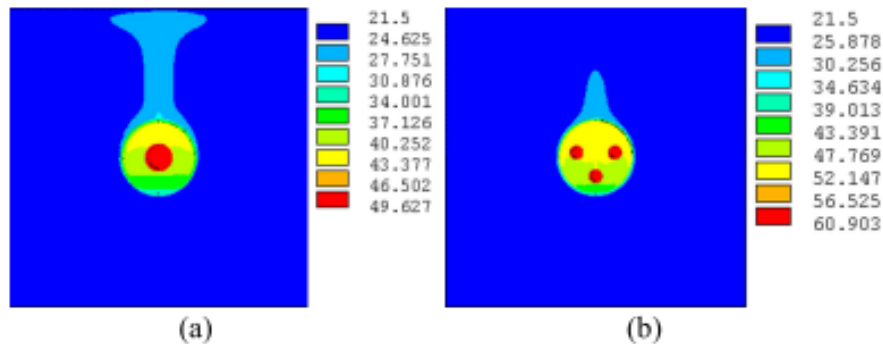


Figure 2.1 Temperature distributions of the solution regions. (a) Single-phase bus bar. (b) Three-phase bus bar.

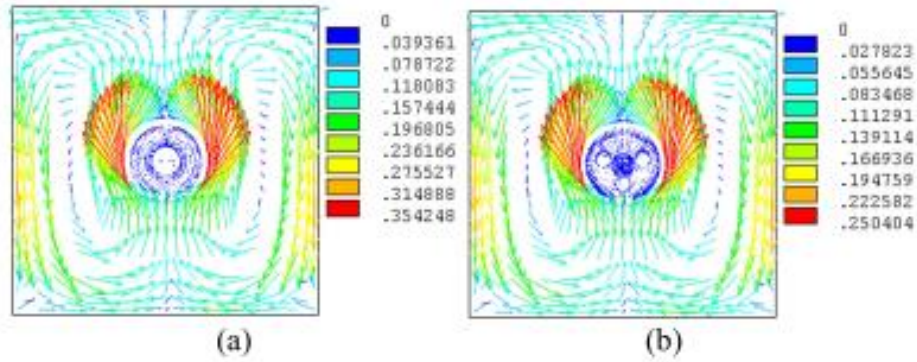


Figure 2.2 Fluid field the solution regions. (a) Single-phase bus bar. (b) Three-phase bus bar.

The fundamental property (stability + consistency = convergence) serves as the basis for the analysis of finite difference schemes [14]. To assess the losses produced in the steel plates and bars, which serve as the sources of heat for the thermal study, a finite element method is proposed by Hwang et al. [15]. For this analysis, a 2-dimensional model is employed, and the method produces good numerical results when compare with test data. Next, Kim et al. [16] proposed a new magnetothermal finite element analysis to estimate the temperature increase of the extra-high voltage gas insulated switchgear bus bar. The thermal analysis's prediction of the temperature rise is based on the power losses of a bus bar computed by the magnetic field analysis. The Nusselt number is applied analytically to the heat-transfer coefficients on the borders while taking into account the material constant and model geometry for natural convection. Figure 2.3 showed the calculated and measured temperature values of the bus bar model. It can be concluded that the coupled magnetothermal finite element analysis's depiction of the temperature distribution in a bus bar is nearly close with the results of the experiments.

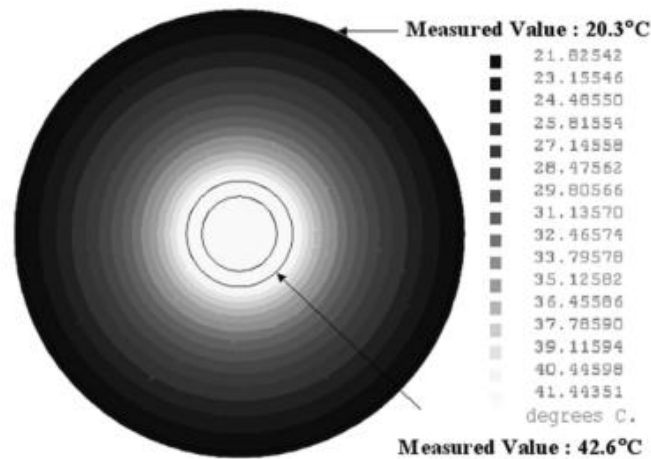


Figure 2.3 Temperature distribution of a single-phase bus bar model

2.5 Finite Volume for Fluid Flow

Ham et al. [17] investigated a finite volume three-dimensional numerical flow field study with various types of bus bars. They found that doing laminar natural convection flow analysis can accurately estimate the temperature rise of a bus bar. Moreover, Zhang et al. [18] used finite volume method (FVM) and mathematical models to analyze the three-dimensional thermal and fluid fields of switch cabinet. The contact areas between the fixed contact and the moving contact are where temperatures rise the fastest, up to a maximum of 73°C. Refer to the study carried out by S.Thirumurugaveerakumar [19], when air blows perpendicular to the bus bar, the temperature rise will be decreased by approximately 45% owing to forced convective heat dissipation, however when air blows parallel to the bus bar, it would be reduced by about 35%. Song et al. [20] demonstrated the steady temperature-rise of the components within a gas insulated switchgear based on FVM and electromagnetic harmonic method. Figure 2.4 illustrated the outcomes of the simulation and experiment are comparable with about 3.99 K is the greatest temperature-rise error. It is expected

that the simplified models, constant material characteristics, and the neglected external airfield are the major causes of calculation mistakes.

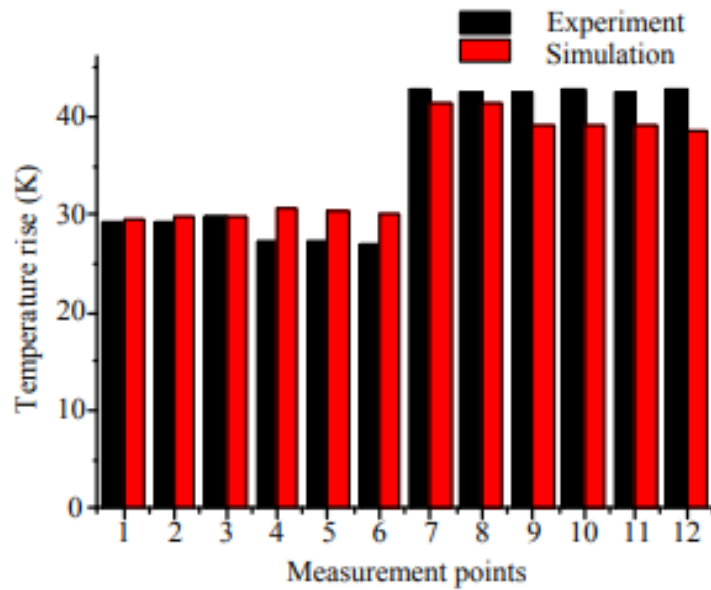


Figure 2.4 Result comparison between experiment and simulations

Douglas V. Nance et al. [21] concluded that FVM accurately enforce boundary constraints over curved borders without the need of convoluted interpolation or interface tracking algorithms. By using the finite volume technique, the spatial discretization scheme may be effectively reduced in order without the requirement to discretize the Laplace operator in generalized coordinates. To determine the distribution of temperature, velocity, and pressure in gas insulated busbar, the finite volume approach is used by Kim et al. [22]. The comparison of observed and simulated temperatures yields findings within 10% of the maximum relative error.

2.6 Bus Duct Design

A research was done by Shadlaghani et al. [23] to investigate numerically the best fin design for a heat sink under forced convection to get a greater heat transfer rate. From Figure 2.5, triangular, rectangular, and trapezoidal fins with constant volume were first investigated. The triangle form was discovered to have a higher heat transmission rate than other shapes. Second, the cross-section of a triangular fin was studied with different perforations as shown in Figure 2.6, and the findings revealed that the heat transfer rate rises as the ratio of fin height to thickness increases. Then, the convection was increased by utilizing longitudinal varied form perforation at various positions. The best design, which produced the highest heat transfer rate, was found to be rectangular perforation with 0.3 (H_c/H) position.

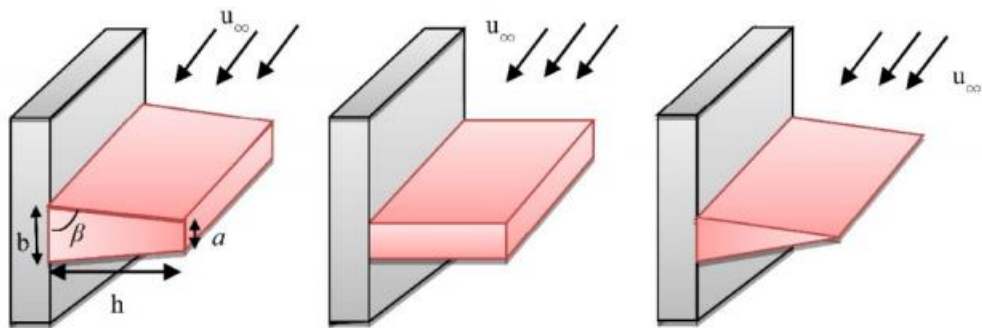


Figure 2.5 Fins with different geometrics [23]

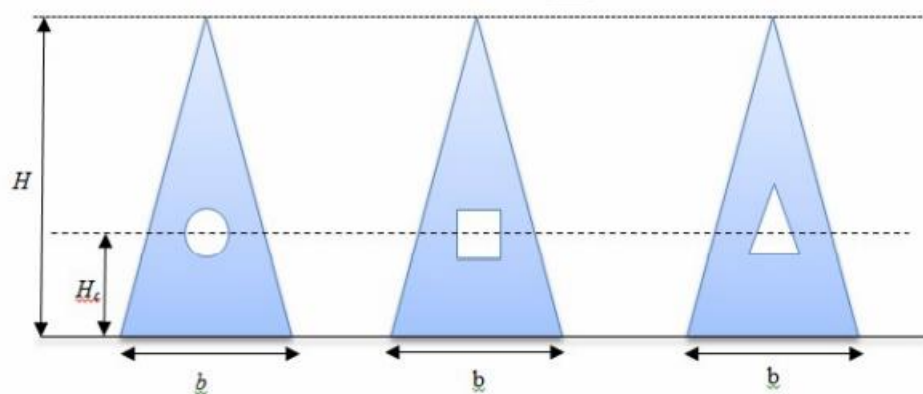


Figure 2.6 Schema of triangular fin along with the different perforations [23]

In the other hand, the effects of short-circuit current on electromagnetic forces in rectangular busbar systems have been investigated using the Maxwell Stress technique by Farhana Mohamad Yusop et al. [24]. The stronger the electromagnetic force, the larger the short-circuit current. The effects of various conductor busbar dimensional arrangements on the maximum value of electromagnetic force were explored. By increasing the conductor thickness and distance between neighbouring conductors by 1mm, the magnitude electromagnetic force was lowered by around 4% to 7%.

A research was carried out by M. J. Kim et al. [25] to improve energy efficiency by improving the geometry of the busbar and the surface treatment on the busbar. Using electromagnetic and thermal analysis, the appropriate thickness of the tunnel-type busbar and the spacing between busbars in a 3-phase parallel array condition were determined. The busbar created in this work has a maximum surface temperature roughly 8 °C lower than a normal plate-type busbar. Second, using a thermal imaging camera and a hot plate, it was proven that the BN-coated Cu had the lowest surface temperature and substrate temperature among the three specimens. The difference in internal temperature between uncoated Cu and BN-coated Cu measured using a hot plate was 19.4 °C. It is thought that by using the produced busbar in this research, energy loss owing to heat production in the switchboard may be decreased.

Besides that, Kobus et al. [26] conducted a thorough study of the thermal performance of a pin-fin heat sink while also developing a rigorous theoretical model capable of predicting the thermal performance of different heat sink geometrical patterns. They discovered that the convective heat transfer coefficient rose as the diameter of the pin reduced. It was also discovered that raising the pitch size near the

natural convection area reduced the fin bundle effect, which increased the convective heat transfer coefficient.

Interruptions, slots, and perforations are some of the frequent geometrical alterations that have been shown to increase the thermal efficiency of fins [27]. Liu et al. [28] also performed theoretical and numerical studies on printed circuit heat exchangers and discovered that a number of design factors, including the lowering the ratio of fin thickness to channel radius, working in an environment with a low convective coefficient, and choice of the fin material, can enhance the effectiveness of the fins. Using materials with thicker fins, lower fluid convective coefficient and better thermal conductivity can improve fin efficiency in a similar manner.

2.7 Summary

A finite element method is a discretization based upon a piecewise representation of the solution in terms of specified basis functions [29] whereas a finite volume method is a discretization based upon an integral form of the PDE to be solved [30]. Most of the research proved that the simulation results are close to the experimental values, that are within 10% of percentage error. However, there is still lack of explanation about effects of fin length and fin valley on the performance of bus duct conductor. Many previous studies related the temperature, heat transfer rate and convective heat transfer coefficient of heatsink with the design of heatsink but it is insufficient to provide thermal performance such as Nusselt Number, temperature contour and velocity contour for further explanation. By understanding the effects of fin length and fin valley on the performance of bus duct conductor, various optimization strategies can be implemented to minimize the cost and improve the heat transfer rate of heatsink in commercial and industrial area.

CHAPTER 3

METHODOLOGY

3.1 Overview

The numerical analysis was carried out using Ansys 2021R. To model the Joule losses from the copper conductor and the impact of convection, conduction, and radiation on the thermal performance of the bus duct system, Ansys Thermal-Electric and Fluent systems were both used. Figure 3.1 depicts the overview of the flow chart of the simulation setup used in the current study.

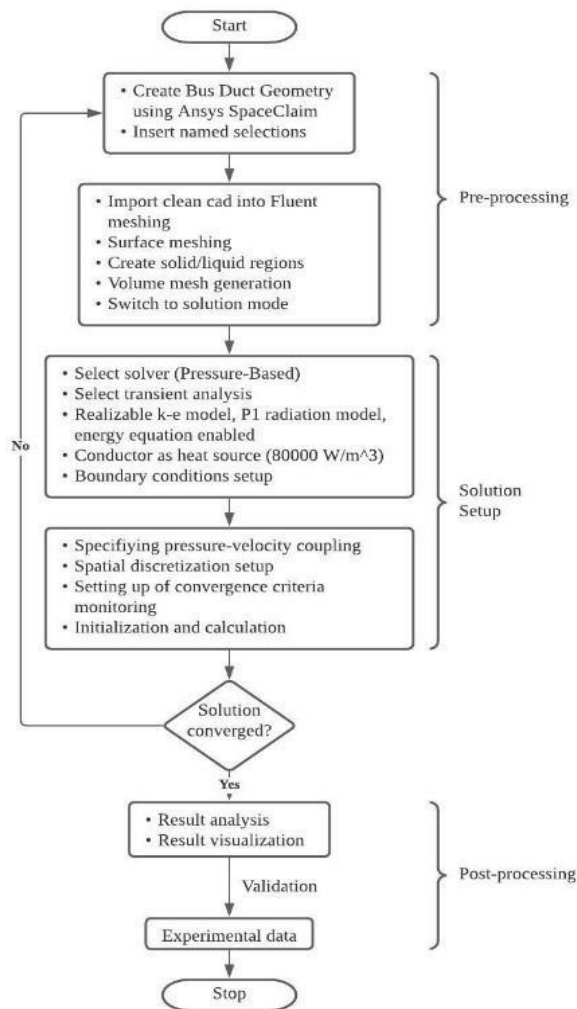


Figure 3.1 Flow chart of simulation setup

3.2 Mathematical Equations

In order to investigate the heat transfer characteristics of the heatsink, a method known as mathematical modelling is used. A physical phenomenon is modelled mathematically by casting one or more differential equations. We will utilise these mathematical equations to depict some aspects of physics, involving the continuity equation, Navier-Stokes equation, energy equations and momentum equation as defined below. The mass conservation equation, or Equation 1, says that matter cannot be created or destroyed. This means the rate of change of mass within the control volume and the mass flux going through the volume's surface are both constant. [31]

$$\rho \left(\frac{du}{dx} + \frac{dv}{dy} + \frac{dw}{dz} \right) = 0 \quad (1)$$

where the local velocity components u , v , and w , which are functions of the point's location as represented by (x, y, z) , and time (t) , describe the fluid velocity V at any point.

$$\frac{du}{dt} + u \frac{du}{dx} + v \frac{du}{dy} + w \frac{du}{dz} = -\frac{1}{\rho} \frac{d\rho}{dx} + \nu \frac{d^2u}{dx^2} + \nu \frac{d^2u}{dy^2} + \nu \frac{d^2u}{dz^2} \quad (2)$$

$$\frac{dv}{dt} + u \frac{dv}{dx} + v \frac{dv}{dy} + w \frac{dv}{dz} = -\frac{1}{\rho} \frac{d\rho}{dx} + \nu \frac{d^2v}{dx^2} + \nu \frac{d^2v}{dy^2} + \nu \frac{d^2v}{dz^2} \quad (3)$$

$$\frac{dw}{dt} + u \frac{dw}{dx} + v \frac{dw}{dy} + w \frac{dw}{dz} = -\frac{1}{\rho} \frac{d\rho}{dx} + \nu \frac{d^2w}{dx^2} + \nu \frac{d^2w}{dy^2} + \nu \frac{d^2w}{dz^2} \quad (4)$$

where the fluid density is ρ and the kinematic viscosity is ν . The Navier-Stokes equations are represented in three dimensions by Equations 2, 3, and 4. These equations explain the relationship between a flowing fluid's physical characteristics, including temperature, velocity, density and pressure. [32][33]

Equation 5 illustrates how Newton's rule of cooling defines the rate of heat transfer from a surface at a particular temperature T_s to the surrounding medium at T_∞ ,

$$\dot{Q}_{conv} = hA_s (T_s - T_\infty) \quad (5)$$

where,

A_s = Heat transfer surface area

h = convection heat transfer coefficient

The volume element of the extended surface (fin) at a particular point x with a length of Δx can be used to obtain the fin equation. The energy balance under steady-state circumstances is represented as follows:

$$\dot{Q}_{cond,x} = \dot{Q}_{cond,x+\Delta x} + \dot{Q}_{conv} \quad (6)$$

where,

$$\dot{Q}_{conv} = h(p \Delta x)(T - T_\infty) \quad (7)$$

The result is obtained by substituting, dividing by Δx , and taking Δx as it approaches zero's limit,

$$\frac{d\dot{Q}_{cond}}{dx} + hp(T_s - T_\infty) = 0 \quad (8)$$

The differential equation regulating heat transport in fins would be represented by equation 9 if Fourier's law of heat conduction were substituted into equation 8.

$$\frac{d}{dx}(KAc \frac{dT}{dx}) - hp(T_s - T_\infty) = 0 \quad (9)$$

The first law of thermodynamics is where the conservation of energy comes from. It claims that the heat added net rate and the work done net rate in a system equals the energy change time rate. Equation 10 represents the conservation of energy equation. Local acceleration is represented by the first term, while advection is represented by the second, third, and fourth terms. The temperature flow resulting from heat conduction is represented by fifth, sixth and seventh terms where k is the thermal conductivity while C_p are the specific heat capacity.

$$\frac{dT}{dt} + u \frac{dT}{dx} + v \frac{dT}{dy} + w \frac{dT}{dz} = -\frac{k}{\rho c_p} \frac{d^2T}{dx^2} + \frac{k}{\rho c_p} \frac{d^2T}{dy^2} + \frac{k}{\rho c_p} \frac{d^2T}{dz^2} \quad (10)$$

When a current is passed through a conductor, heat is produced. This process known as Joule heating, often referred to as resistive heating. One volumetric heat source's heat loss was taken into account as Joule losses. Due to the fact that both heat and electricity were generated, the Thermal-Electric Analysis System was used to determine the heat source's size. The analytical technique was utilised to determine the Joule losses from the bus bar using equations 11 and 12.

$$P_{joule} = I^2 R \quad (11)$$

$$Q = \frac{P_{joule}}{V} \quad (12)$$

$$R = \rho \times \frac{L}{S} \quad (13)$$

where,

Q = heat loss (W/m³)

V = Volume of geometry (m³)

ρ = resistivity (kg·m³·s⁻³·A⁻²)

L = length (m)

S = Cross sectional area (m²)

3.3 Computational Approach

Pre-processing, solution setup, and post-processing were the three separate phases of the simulation.

3.3.1 Pre-processing

The pre-processing stage included two tasks which are designing the bus duct housing according to the specified dimensions and meshing the geometry.

3.3.1(a) Geometrical Model

The geometry was designed using Ansys Spaceclaim based on the exact dimensions of the AH Copper Bus Duct System provided by Furutec Electrical Sdn. Bhd. to be used in the experimental setup. After completion of modeling the bus duct housing, the model was then exported to Fluent meshing for further processing. The bus duct housing model was shown in Figure 3.2.

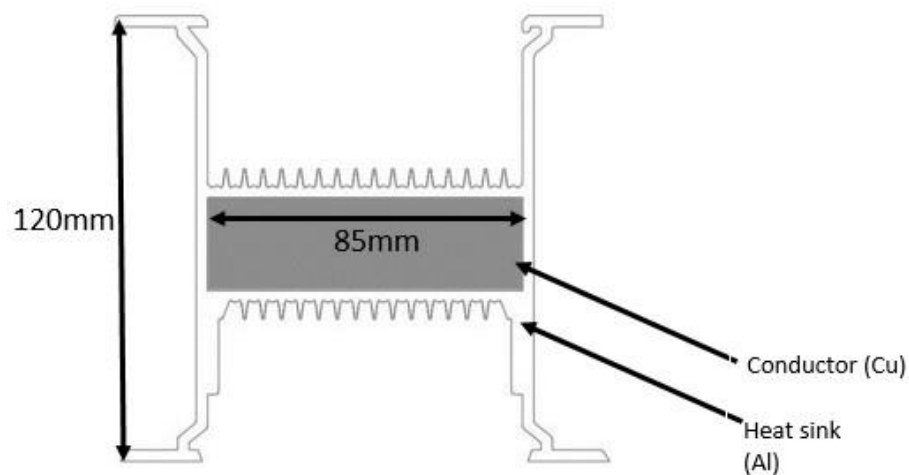
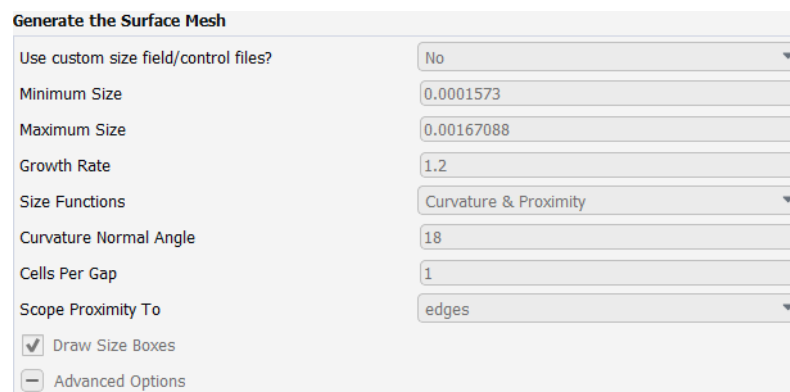


Figure 3.2 Dimension and Geometrical Setup

3.3.1(b) Meshing

Fluent meshing was used to mesh the geometry. The Mesh Independent Test was carried out to ensure that the simulation results were independent of the mesh resolution. A mesh that was too fine could need more processing resources while a mesh that was too coarse might not yield correct results. Therefore, it was crucial to perform the Mesh Independent Test in order to determine the ideal mesh size and prevent inaccurate findings. Similar mesh sizes may be used for the additional simulation experiments after the most optimal mesh size had been identified. The detail of mesh independent study will be explained in Chapter 4.1.

Based on Figure 3.3, poly-hexcore combined disparate meshes with polyhedral elements. The curvature and proximity size functions were chosen, and the minimum surface mesh size was set at 0.0001573 with a growth rate of 1.2. Boundary layers were added to the fluid domain.



Generate the Surface Mesh	
Use custom size field/control files?	No
Minimum Size	0.0001573
Maximum Size	0.00167088
Growth Rate	1.2
Size Functions	Curvature & Proximity
Curvature Normal Angle	18
Cells Per Gap	1
Scope Proximity To	edges
<input checked="" type="checkbox"/> Draw Size Boxes	
<input type="checkbox"/> Advanced Options	

Figure 3.3 Surface mesh setup showing minimum surface mesh size was set at 0.0001573 with a growth rate of 1.2

Next, three boundary layers with a transition ratio of 0.272 and a growth rate of 1.2 were included. Figure 3.4 showed the volume mesh was filled with poly-hexcore cells with a minimum and maximum cell length of 0.0001573 and 0.0025168, respectively. The total number of elements was approximately 1.4 million. The results of meshing was shown in Figure 3.5.

Generate the Volume Mesh

Fill With	poly-hexcore
<input checked="" type="checkbox"/> Mesh Solid Regions	
Buffer Layers	2
Peel Layers	1
Min Cell Length	0.0001573
Max Cell Length	0.0025168
<input type="checkbox"/> Region-based Sizing	
<input checked="" type="checkbox"/> Enable Parallel Meshing	
<input type="checkbox"/> Advanced Options	
Use Size Field?	no
Polyhedral Mesh Feature Angle	30
Avoid 1/8 octree transition?	no
Fill Polyhedra in solids?	no
Quality Improve Limit	0.05
Check Self Proximity	yes

Figure 3.4 Volume mesh setup showing the volume mesh is filled with poly-hexcore cells

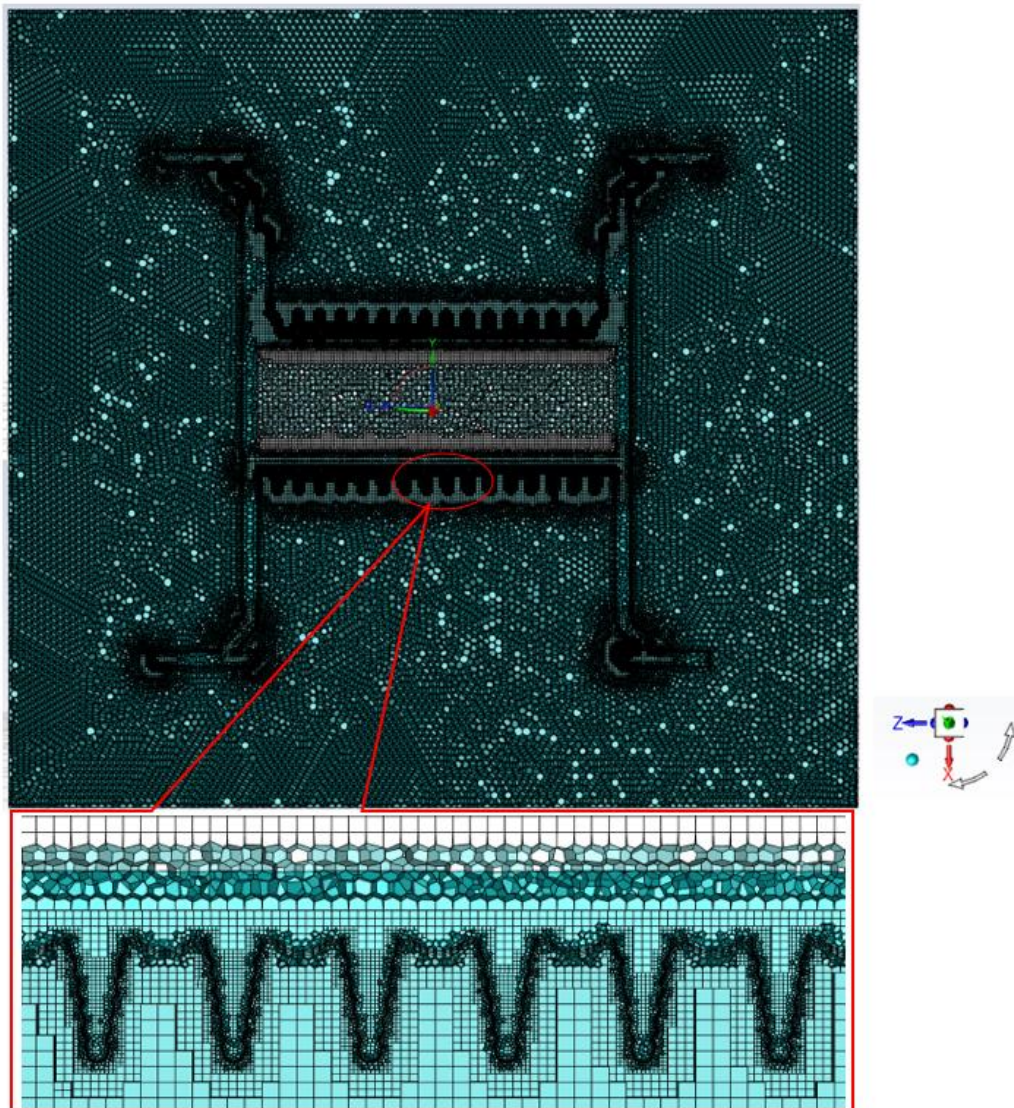


Figure 3.5 Mesh grid and three boundary layers details around heat sink

3.3.2 Computational Setup

The transient approach was used to carry out the simulation study as shown in Figure 3.6. This was because of the relatively large temperature changes in the simulation domain. Due to Joule heating, the temperature of conductor was typically 90°C, while the fluid domain's working temperature was 30°C. The mass inside the simulation domain had a significant impact on the solution when simulating natural convection. However, this mass is unknown unless the density is taken into account before the simulation. Therefore, by using the starting pressure and temperature, the transient technique enables the initial density to be calculated.

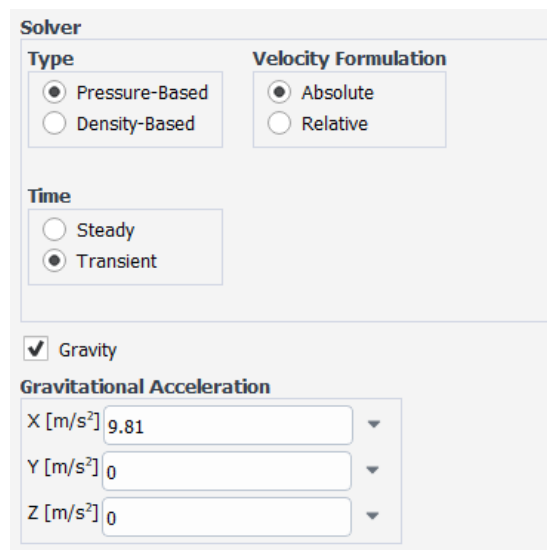


Figure 3.6 General setup showing pressure-based solver with transient time

The pressure-based solver and realizable k-e model as viscous model were used to predict the spreading rate of both planar and round jets more accurately. Additionally, there was a greater probability that this model will perform better for flows that involved rotation, boundary layers subjected to significant pressure gradients, separation, and recirculation. The P1 radiation model was used in the simulation setup to accurately model radiation while using less computer resources. The P1 type

performed admirably in situations requiring significant optical thickness. The fluid domain and the heat sink participated in the radiation heat transfer.

The pressure-based solver used PRESTO! as the spatial discretization technique. PRESTO! was typically chosen for natural convection and buoyancy-driven flows as well as flows with a high Rayleigh number of natural convections. The second-order upwind discrimination scheme was used to attain higher-order accuracy at the cell faces to increase the accuracy of the results. The Taylor series expansion about the element's cell centroid was used in this scheme.

3.3.2(a) Boundary Conditions Setup

The simulation model's cell zone and boundary conditions were shown in Figure 3.7. The conductor, heatsink, and fluid domain were the three separate cell zones in this arrangement. In this investigation, the copper conductor's Joule losses served as the primary source of heat. The current was set at 1500A. According to Equation 11, the Joules losses was calculated as the square of the current times the electrical resistance for the conductor length. A simplified analytical calculation with the assumption of a direct current running through the conductor and neglected for skin and proximity effects produced a Joule loss of 80000 Wm^{-3} . The material of conductor was set as copper with thermal conductivity of 387.6 W/mK and an internal emissivity coefficient of 0.05. With Ansys Fluent's default settings, the fluid domain was defined to be air. The heat sink, in comparison, was made of aluminium with an internal emissivity coefficient of 0.09 and thermal conductivity of 202.4 W/mK . In order to mimic natural convection and guarantee that no aspects of forced convection were impacting the simulation domain, the fluid domain had four outputs with gauge pressures of 0 Pa. The operating temperature was set to 30°C , operating pressure was set to 101325 Pa, and operating density was set to 1.225 kg/m^3 .

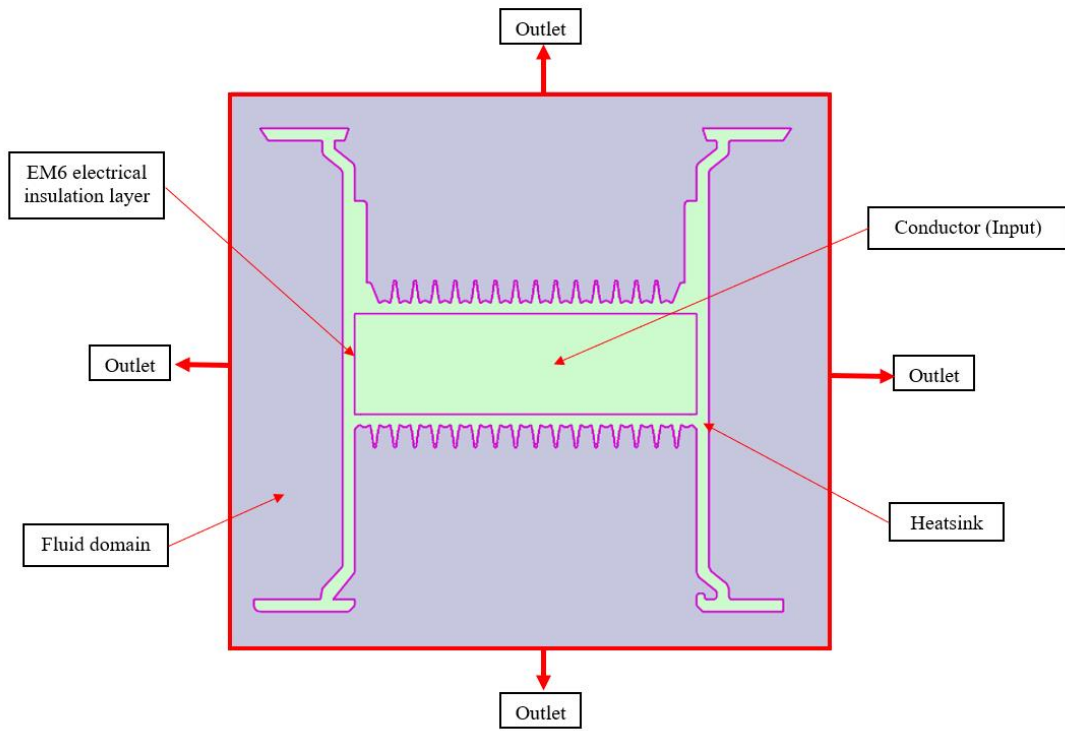


Figure 3.7 Boundary conditions and cell zone conditions

3.3.2(b) Run Calculation Setup

Gravitational acceleration was enabled in the positive-X direction with a value of 9.81 ms^{-2} . The simulation was initialized using the standard method with the initial temperature set to 30°C . Figure 3.8 illustrated a time step of 0.1 second and a 20000 number of time steps were used to model the heat transfer until steady-state with no temperature changes on the heat sink. Before running the simulation, create an automatic export with flow time of 200 seconds for post-processing use.

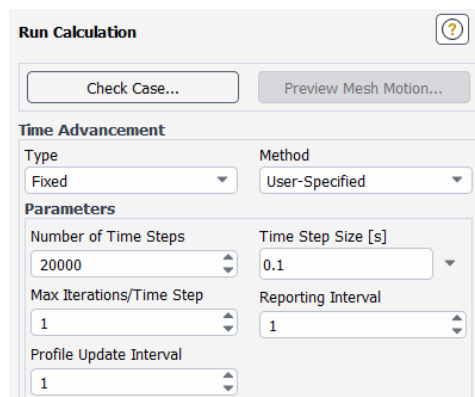


Figure 3.8 Run calculation setup showing the parameter with 20000 time steps and 0.1 time step size

3.3.3 Post-processing

In this stage, post-processing was carried out to find the thermal performance of heatsink such as total heat transfer rate, average surface heat transfer coefficient, average surface temperature and average surface Nusselt number. The temperature contour and velocity contour of heatsink were also obtained for further discussion.

3.3.3(a) Thermal Performance of Heatsink

After the simulation was done, “Solution” was clicked from the Workbench. From the “Results”, “Reports” was clicked to choose “Fluxes”. From the flux report, “Total Heat Transfer Rate” was selected and then “fluid-domain-heatsink” was filtered to choose the shadow as demonstrated in Figure 3.9.

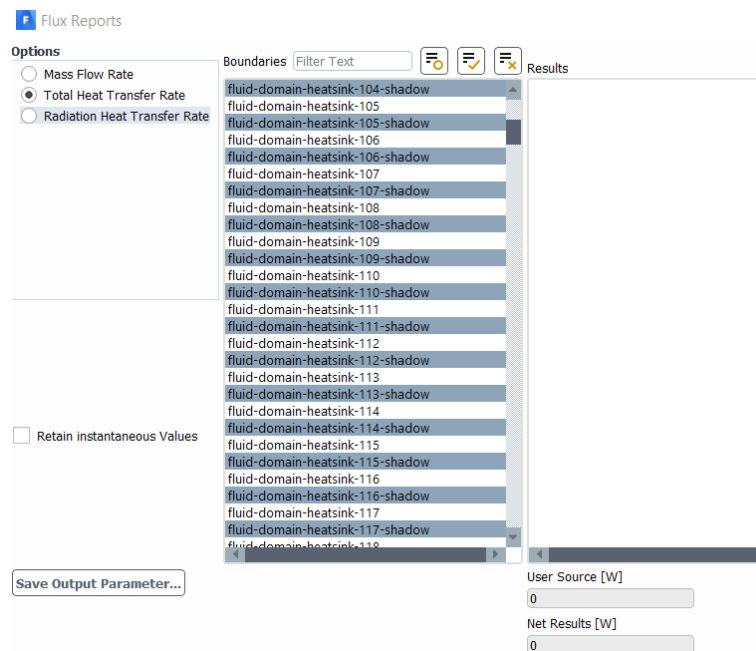


Figure 3.9 Flux reports showing total heat transfer rate was chosen and “fluid-domain-heatsink” was filtered to choose the shadow.

“Wall” was clicked from “Boundary Conditions” to double confirm the fluid-domain-heatsink-shadow are the correct chosen as heatsink highlighted in Figure 3.10. Adjacent cell zone was heatsink meaning the heat transfer was from the surface of heatsink which was what we wanted. Then, the result was computed, copied, and paste